Singular patterns for an aggregation model with a confining potential

T. Kolokolnikov, Y. Huang and M. Pavlovski

February 27, 2012

Abstract. We consider the aggregation equation with an attractive-repulsive force law. Recent studies [T. Kolokolnikov et.al, PRE 015203R(2011); J.von Brecht et.al, M3AS to appear; D. Balague et.al., preprint] have demonstrated that this system exhibits a very rich solution structure, including steady states consisting of rings, spots, annuli, N-fold symmetries, soccer-ball patterns etc. We show that many of these patterns can be understood as singular perturbations off lower-dimensional equilibrium states. For example, an annulus is a bifurcation from a ring; soccer-ball patterns bifurcate off solutions that consist of delta-point concentrations. We apply asymptotic methods to classify the form and stability of many of these patterns. To characterize spot solutions, a class of "semi-linear" aggregation problems is derived, where the repulsion is described by a nonlinear term and the attraction is linear but non-symmetric. For a special class of perturbations that consists of a Newtonial repulsion, the spot shape is shown to be an ellipse whose precise dimensions are determined via a complex variable methods. For annular shapes, their width and radial density profile are described using perturbation techniques.

1 Introduction

Collective group behaviour is a fascinating natural phenomenon that is observed at all levels of the animal kingdom, from beautiful bacterial colonies, insect swarms, fish schools and flocks of birds, to complex human population patterns. The emergence of very complex behaviour is often a consequence of individuals following very simple rules, without any external coordination. In recent years, many models of group behaviour have been proposed that involve nonlocal interactions between the species [2, 10, 11, 23, 24, 26]. Related models also arise in other important applications such as self-assembly of nanoparticles [19, 20], theory of granular gases [27], invasion models [13], chemotaxic motion [14, 18], and molecular dynamics simulations of matter [17].

One of the simplest models of insect swarming was proposed in [24]. In this model, each individual is represented by a particle moving in space. Every particle A "feels" every other particle B through a force whose magnitude $F(r)$ depends only on the pairwise distance between the two particles and which acts in the direction from A to B. Each particle then moves in the direction of the average force acting upon it. These simple assumptions lead to an *aggregation model* for a system of particles located at $\{x_1, \ldots, x_N\}$,

$$\frac{d}{dt}x_k = \frac{1}{N}\sum_{j \neq k} F(|x_k - x_j|)\frac{x_k - x_j}{|x_k - x_j|}, \qquad k = 1, \ldots, N. \tag{1}$$

The force law $F(r)$ is assumed to *repulsive at short distances* (i.e. $F(r) > 0$ for small r) and *attractive at large distances* (i.e. $F(r) < 0$ for sufficiently large r). For convenience, we will often use the notation

$$\frac{d}{dt}x_k = \frac{1}{N}\sum_{j \neq k} f(|x_k - x_j|)\,(x_k - x_j), \qquad k = 1, \ldots, N, \tag{2}$$

where $f(r) = F(r)/r$. The continuum limit $N \to \infty$ of (2) yields the system [4],

$$\rho_t + \nabla \cdot (v\rho) = 0; \qquad v = \int_{\mathbb{R}^d} f(|x - y|)(x - y)dy. \tag{3}$$

The aggregation model (3) and its discrete analogue (2) have been intensively studied over the past decade and by now a vast literature exists on this topic; see for example [1, 4, 5, 6, 7, 8, 15, 16, 21, 24, 26, 28, 29] and references therein. There are also many studies of related second-order models that incorporate acceleration of self-propelled particles; see for instance [9, 12, 22] and references therein.

In a series of papers [21, 28, 29, 1], the authors have investigated a very rich solution structure for a family of such attractive-repulsive force laws. A particularly simple solution in two dimensions consists of a *ring*, where the particles align themselves along a circular ring uniformly. Another type of a simple solution consists of *clusters* of particles, whereby the equilibrium state consists of K "holes", with each particle belonging to one of such holes. The stability of cluster solutions in one dimension was characterized in [15]; we will extend this analysis to higher dimensions in §2 below.

To illustrate the large variety of possible steady states, consider the "piecewise-linear" force

$$F(r) = \min\left(ar + b, 1 - r\right), \quad 0 \leq b \leq 1. \tag{4}$$

As shown on Figure 1, this family generates a rich equilibrium structure that is very sensitive to the choice of parameters a and b. Note in particular the presence of "spot" solutions, such as when $(a, b) = (0.8,\ 0.05)$; and the annulus solutions such as when $(a, b) = (0.4, 0.15)$. Such solutions are prevalent in numerical simulations, and typically bifurcate from simpler ring or cluster solutions[1]. The main goal of this paper is to study these more complex solutions including annuli, spots, and "soccer balls".

---

[1]In [21], the family $F(r) = b + \tanh\left((1 - r)a\right)$ was shown to also generate a wide variety of steady states, many similar to what is shown in Figure 1.
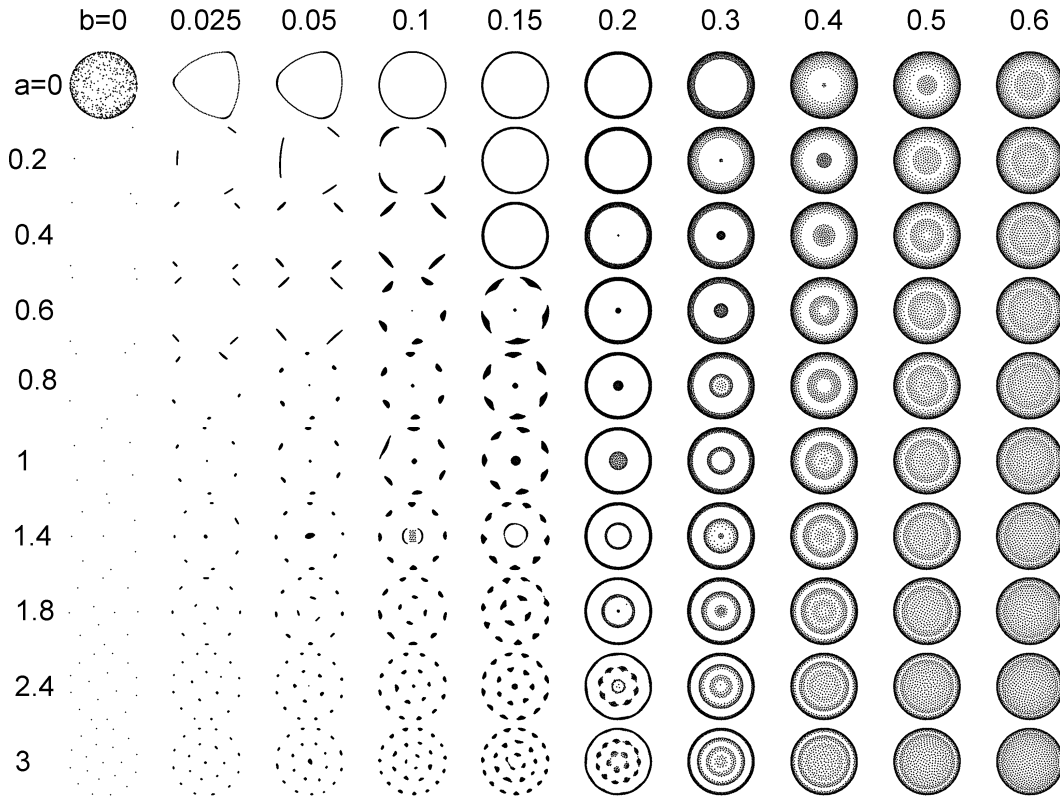
b=0   0.025   0.05   0.1   0.15   0.2   0.3   0.4   0.5   0.6

a=0
0.2
0.4
0.6
0.8
1
1.4
1.8
2.4
3

Figure 1: Steady states of (1) with $F(r) = \min\left(ar + b, 1 - r\right),$ using $N = 1000$ particles and with a, b as indicated. A snapshot at $t = 10,000$ is shown. Integration was performed using forward Euler method with stepsize 0.5.

Let us now summarize our findings. We start by extending the work of [15] on point clusters to two and higher dimensions in §2. Such clusters can occur when the repulsion near the origin is weak, $F(0) = 0$. On the other hand, when the repulsion at small distances is small but positive, $0 < F(0) \ll 1$, the holes "degenerate" into small spots. In §3 we derive the reduced canonical problem (30) that describes the shape of a single spot. This reduced problem depends only on two parameters and is analysed in §3. There are two basic steady states of the reduced problem (30): the simplest steady state consists of particles along a line; such steady states appear for in Figure 1 with $(a, b) = (0.2, 0.025)$. A more complex shape is a fully-two dimensional steady state such as e.g. $(a, b) = (0.8, 0.05)$. We fully characterize the stability of the former in terms of Harmonic numbers (see Theorem 3.2). Using the results of [8] also shows that the steady states are bounded in the continuum limit. In §3.2 we extend the analysis for the case where a small amount of Newtonian repulsion is added to the kernel. The resulting spots have a constant density and their shape is an ellipse whose axes are completely characterized in terms of the
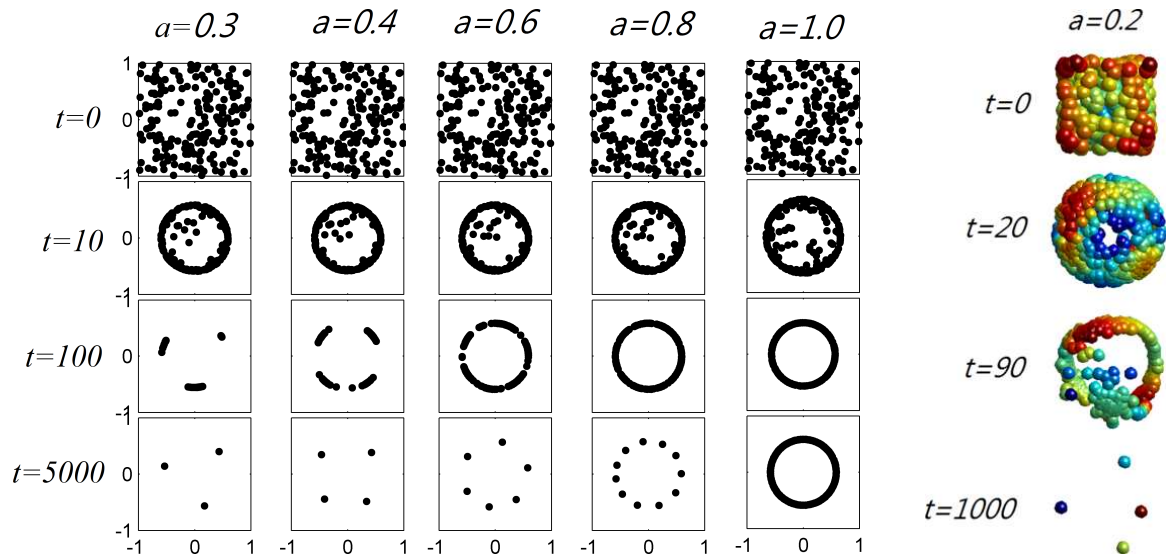
3

Figure 2: Snapshots of solution to (2) with $N = 500$, $f(r) = \min(a, 1 - r)$ and with a and t as indicated, starting with random initial conditions inside a unit square. Left pane shows computations in $\mathbb{R}^2$; right pane is the same computation in $\mathbb{R}^3$.

original kernel (see Theorem 3.3 for details).

In §4 we turn our attention annular solutions such as in Figure 1 with $(a, b) = (0.4, 0.15)$. These arise as singular perturbations of the ring solutions, when the ring solution is ill-posed, in the sense that it is unstable to very high modes (see [21] for more details). In the Main Result 4.1 we describe the radial density profile within the annulus, as well as its width. We show that in the continuum limit the density blows up at the edges of the annulus; see Figure 5 for an illustration. In §4.1 we examine the annulus that results when a small Newtonian repulsion is added. In this case, the resulting annulus has uniform density and we explicitly compute its dimensions; see Figure 6 for an example. We conclude the paper with discussion and open problems in §5.

2   Solutions consisting of point concentrations

When the repulsion force $F(r)$ is sufficiently weak near the origin, the particles may coalesce as $t \to \infty$, so that in the large particle limit, a steady state can emerge which consist of K points, where K is independent of the number of particles $N \to \infty$. An example of such evolution is illustrated in Figure 2; such steady state also occurs in Figure 1 with $b = 0$. This behaviour can occur when $F(r) \to 0^+$ as $r \to 0^+$. In terms of the function $f(r) = F(r)/r$ in (2), we will assume that

$$f(0) = a; \quad f(r) \text{ is continuous for } r \geq 0. \tag{5}$$

4

A simple such function which we will study in detail below is given by

$$f(r) = \min(a, 1 - r). \qquad (6)$$

From (2), the boundedness of $f(r)$ at the origin implies that the repulsion is small at small distances; this can cause the particles to collide to form "black holes" as $t \to \infty$. In the limit $N \to \infty$, the steady state then consists of a union of point delta-concentrations. In one dimension, such solutions and their stability were studied in detail in [15] using the continuum formulation. In this section, we start by extending their theory to two and higher dimensions. When $a > 0$, in dimension d, the minimum possibly stable configuration is $K = d + 1$ such holes[2].

For notational simplicity, we will consider a solution consisting of K equal holes, so that each hole contains precisely $n = N/K$ particles. We then rewrite (2) as

$$x'_{k,l} = \frac{1}{N} \sum_{g,j} f\left(|x_{k,l} - x_{g,j}|\right) (x_{k,l} - x_{g,j}), \qquad k, g \in \{1, 2, \ldots K\}; \quad l, j \in \{1, 2, \ldots n\}. \quad (7)$$

The first index refers to the hole number while the second index refers to the particle number inside that hole. The steady state of (7) is simply

$$x_{k,l} = x_k, \quad k = 1 \ldots K, \quad l = 1 \ldots n \qquad (8)$$

with x_k satisfying

$$0 = \sum_j f(|x_k - x_j|)(x_k - x_j), \qquad k = 1 \ldots K. \qquad (9)$$

We now study the local stability of K holes. Linearization around the steady state takes the form

$$x_{k,l}(t) = x_k + \phi_{k,l}(t); \qquad |\phi_{k,l}| \ll 1, \quad k = 1, \ldots, K, \quad l = 1, \ldots, n,$$

leading to

$$\frac{d}{dt}\phi_{k,l} = \frac{1}{N} \sum_{g,j} \frac{f'\left(|x_k - x_g|\right)(x_k - x_g) \cdot (\phi_{k,l} - \phi_{g,j})}{|x_k - x_g|} (x_k - x_g)$$
$$+ \frac{1}{N} \sum_{g,j} f\left(|x_k - x_g|\right)(\phi_{k,l} - \phi_{g,j}). \qquad (10)$$

In $\mathbb{R}^d$, this is dN dimensional linear system. To study the stability of this system, its solution space is decoupled into two subspaces:

Subspace A: $\sum_l \phi_{k,l} = 0, \quad k = 1 \ldots K$;

Subspace B: $\phi_{k,l} = \phi_k, \quad k = 1 \ldots K; \; l = 1 \ldots n.$

---

[2]For example in two dimensions, two holes are necessary unstable, as there is nothing to counteract the weak repulsion in the direction perpendicular to the line through the two holes.

Note that these two subspaces have zero intersection. Moreover, dimension of subspace A is $dN - dK$ whereas the dimension of subspace B is dK; so together they span the entire solution space of dimension dN. Subspace A leads to a self-consistent system

$$\frac{d}{dt}\phi_{k,l} = \frac{1}{K}M_k\phi_{k,l} \tag{11}$$

where M_k is a $d \times d$ matrix given by

$$M_k := aI + \sum_{g \neq k}\left[\frac{f'(|x_k - x_g|)}{|x_k - x_g|}(x_k - x_g) \otimes (x_k - x_g) + f(|x_k - x_g|)I\right]. \tag{12}$$

where $a = f(0)$, I is the $d \times d$ identity matrix, and $\otimes$ is the vector tensor product, i.e. $v \otimes w = vw^T$ is the matrix whose i,j-th entry is v_iw_j.

The subspace B leads to the system

$$\frac{d}{dt}\phi_k = \frac{1}{K}\sum_{g \neq k}\left(\frac{f'(|x_k - x_g|)(x_k - x_g)\cdot(\phi_k - \phi_g)}{|x_k - x_g|}(x_k - x_g) + f(|x_k - x_g|)(\phi_k - \phi_g)\right). \tag{13}$$

The problem corresponding to subspace B is equivalent to the stability of K holes when each hole has only one particle inside. We can thus state the following result.

Proposition 2.1 *Suppose that $f(r)$ is bounded near the origin and consider a steady state of (7) consisting of K holes as given by (9). It is stable if and only if the following two conditions are satisfied:*

(i) The steady state is stable when each of the holes contains only one particle (i.e. $n = 1, \quad N = K$);

(ii) The K matrices $M_k \in \mathbb{R}^{d \times d}$ defined by (12) are all negative semidefinite.

An important special case in $\mathbb{R}^2$ for which a fully explicit computation is possible is when x_k are uniformly located along a ring of some radius r; that is

$$x_k = r_0 \exp\left(2\pi i k/K\right), \qquad k = 1, 2, \ldots, K.$$

In this case the radius r_0 satisfies (9)

$$\sum_{g=1}^{K-1} f\left(2r_0 \sin(\pi g/K)\right)\sin^2(\pi g/K) = 0. \tag{14}$$

When $n = 1$, i.e. case (i) of Proposition 2.1, the stability of K particles was fully characterised in [21]. It was shown that $n = 1$ case is stable provided that a sequence of matrices $M(m)$, $m = 0, \ldots, K - 1$ are negative semidefinite, where

6

$$M(m) := \sum_{g=0}^{K-1} \begin{pmatrix} G_2\left(\frac{g\pi}{K}\right)\left[1 - e^{2\pi i(m+1)g/K}\right] & G_1\left(\frac{g\pi}{K}\right)\left[e^{2\pi i(m+1)g/K} - e^{4\pi ig/K}\right] \\ G_1\left(\frac{g\pi}{K}\right)\left[e^{2\pi i(m+1)g/K} - e^{4\pi ig/K}\right] & G_2\left(\frac{g\pi}{K}\right)\left[1 - e^{2\pi i(-m+1)g/K}\right] \end{pmatrix} \quad (15)$$

where we define

$$G_1(\theta) := r_0 f'\left(2r_0 |\sin\theta|\right)|\sin\theta|; \quad G_2(\theta) := G_1(\theta) + f\left(2r_0|\sin\theta|\right). \quad (16)$$

For the subspace A, we note that (11) is a sequence of K *decoupled* problems, each of them a d-dimensional linear system. Moreover, in the case of a ring of holes, by symmetry, the K problems (11) are identical and we write $M_k = \hat{M}$ where after some computations we find that

$$\hat{M} = \begin{pmatrix} -\alpha & 0 \\ 0 & -\beta \end{pmatrix};$$

where

$$\alpha := -a - \sum_{g=1}^{K-1}\left(2G_1(\pi g/K)\sin^2(\pi g/K) + f(2r_0\sin(\pi g/K))\right), \quad (17)$$

$$\beta := -a - \sum_{g=1}^{K-1}\left(2G_1(\pi g/K)\cos^2(\pi g/K) + f(2r_0\sin(\pi g/K))\right), \quad (18)$$

with $a = f(0)$. We summarize the results as follows:

Theorem 2.2 (K equal holes on a ring) *Suppose that $f(r)$ is bounded for small r. Consider the steady state consisting of K delta point concentrations along a ring of radius r_0 given by (14), each containing $n = N/K$ particles. Such state is locally stable if and only $\alpha \geq 0, \beta \geq 0$ and the matrices $M(m)$, $m = 0, \ldots, K-1$ given by (15) are all negative semidefinite.*

We now specialize this theorem further. For the case of three holes we have the following.

Corollary 2.3 *Let $F(r)$ be a C^1 repulsive-attractive force with $F(0) = 0$, $F(d) = 0$, $F(r) \gtrless 0$ for $r \lessgtr d$. Consider a steady state consisting of three equal holes $K = 3$ that form an equilateral triangle in $\mathbb{R}^2$ of size d. Such steady state is locally stable if and only if $2F'(0) \leq -F'(d)$.*

Proof. We have $d = \sqrt{3}r_0$. Recalling that $f(r) = F(r)/r$ we compute $\alpha = -F'(0) - \frac{3}{2}F'(d)$; $\beta = -F'(0) - \frac{1}{2}F'(d)$. Thus the subspace A is stable when $2F'(0) \leq -F'(d)$ with the borderline case $2F'(0) = -F'(d)$ corresponding to $\beta = 0$. On the other hand, the

subspace B is always stable as can be seen by the following energy argument. Consider the energy

$$E = \sum_{k=1}^{3} \sum_{g=1}^{3} P(|x_k - x_g|)$$

where $P'(r) = -F(r)$. Since $F(r)$ has a root at $r = d$, it immediately follows that the triangle whose vertices are at a distance d from each-other is a (local) minimum of E. Since the system (1) with $N = 3$ is the gradient flow of E, it follows that the triangle is a locally stable configuration which proves the stability of the subspace B. ∎

Example. Take $f(r)$ as in (6); the numerical simulations for various values of a of (2) are shown in Figure 2. We now show that the K hole solution is guaranteed to be stable if $a \in (a_1, a_2)$ whose values are summarized in the following table:

K	r_0	a_1	a_2
3	0.577350	0	0.5
4	0.585786	0.171573	0.656851
5	0.587785	0.309017	0.736067
6	0.588457	0.411543	0.788636
7	0.588735	0.489115	0.819194
$\gg 1$	$\frac{3}{16}\pi$	$1 - \frac{3\pi^2}{8K}$	$1 - \frac{\pi^2}{8K}$

$$\tag{19}$$

The value a_1 given in the table corresponds to the minimum possible value of a for which $f(d) = 1 - d = a$, where d is the minimum distance between the two holes, $d = 2r_0 \sin \pi/K$:

$$a_1 = 1 - 2r \sin \pi/K. \tag{20}$$

The matrices $M(m)$ are all negative semidefinite as was shown in [21]. Using identities

$$\sum_{g=1}^{K-1} \sin(\pi g/K) = \frac{\sin \pi/K}{1 - \cos \pi/K}; \quad \sum_{g=1}^{K-1} \sin^3(\pi g/K) = \frac{(1 + \cos \pi/K)^2}{\sin \pi/K \, (1 + 2\cos \pi/K)} \tag{21}$$

and (14) we compute

$$r_0 = \frac{K}{4} \frac{\sin \pi/K \, (1 + 2\cos \pi/K)}{(1 + \cos \pi/K)^2}; \tag{22}$$

$$\alpha = -a + 2r \frac{\sin \pi/K}{1 - \cos \pi/K} - \frac{K}{2} + 1; \quad \beta = -a + 4r \frac{\sin \pi/K}{1 - \cos \pi/K} - \frac{3}{2}K + 1. \tag{23}$$

The threshold a_2 for K holes corresponds to $\beta = 0$:

$$a_2 = 4r_0 \frac{\sin \pi/K}{1 - \cos \pi/K} - \frac{3}{2}K + 1; \tag{24}$$

direct computation shows that $\alpha > 0$ whenever $a \in (a_1, a_2)$. For large K and with $a > a_1$, we have the asymptotics

$$r_0 \sim \frac{3\pi}{16}, \quad a_1 \sim 1 - \frac{3\pi^2}{8K}, \quad a_2 \sim 1 - \frac{\pi^2}{8K} \text{ as } K \to \infty. \tag{25}$$

8

For example, Figure 2, column 4 shows the numerical simulation with $a = 0.6$, starting with random initial conditions, leading to a steady state consisting of 6 holes. This is consistent with our theory: from (19) we surmise that K holes are locally stable where K is any number from 4 to 9.

Pyramid in $\mathbb{R}^3$. Our last example is a *pyramid* in three dimensions. The pyramid consists of $K = 4$ holes located such that the distance between any two holes is d with $F(d) = 0$. In particular we take $x_k = p\left(\cos(2\pi k/3), \sin(2\pi k/3), 0\right)$; $k = 1\ldots 3$ and $x_4 = (0, 0, q)$; with $p\left|(\exp(2\pi i/3) - 1)\right| = d$; $p^2 + q^2 = d^2$ so that $p = \sqrt{1/3}d$; $q = \sqrt{2/3}d$. We then compute

$$M_4 = F'(0) + F'(d) \begin{pmatrix} 1/2 & 0 & 0 \\ 0 & 1/2 & 0 \\ 0 & 0 & 2 \end{pmatrix}.$$

By symmetry, eigenvalues of the matrices M_k are the same for all $k = 1\ldots 4$. This shows that the subspace A is stable if and only if $2F'(0) \leq -F'(d)$. On the other hand, the subspace B is always stable for the pyramid as seen using the energy argument in the proof of Corollary 2.3. We summarize:

Corollary 2.4 *Let $F(r)$ be a C^1 repulsive-attractive force with $F(0) = 0$, $F(d) = 0$, $F(r) \gtrless 0$ for $r \lessgtr d$. Consider a steady state consisting of four equal holes $K = 4$ that form a pyramid in $\mathbb{R}^3$ whose vertices are all distance d apart. Such steady state is locally stable if and only if $2F'(0) \leq -F'(d)$.*

3   Spot solutions

As was shown in §2, cluster solutions occur when the interaction force $F(r)$ vanishes at the origin. In this section, we study what happens to such solutions when the force law has a slight but strictly positive repulsion at the origin, namely

$$F(r) = \delta \quad \text{with} \quad 0 < \delta \ll 1 \ \text{ and } a := F'(0) > 0. \tag{26}$$

In terms of $f(r) = F(r)/r$, this implies the near-distance singular behaviour of the form

$$f(r) \sim \frac{\delta}{r} + a + O(r) \quad \text{as} \ \ r \to 0. \tag{27}$$

As in §2, we will use the double index notation $x_{k,l}$ for particle positions, with first index indicating the spot number $k = 1, \ldots, K$ and the second index indicating the particle inside spot $k : l = 1, \ldots, n$. We are interested in the limit $\delta \ll 0$. When $\delta = 0$, the spot collapses into a hole with $x_{k,l} = x_k$ satisfying (9).

For small but positive δ, numerics indicate that the shape of the spot scales with δ while the overall shape is preserved. For K symmetric spots along a ring, this suggests an anzatz

$$x_{k,l}(t) = x_k + \delta \cdot \phi_{k,l}(t), \qquad \delta \ll 1. \tag{28}$$

In addition, we will assume the self-consistent anzatz $\sum_l \phi_{k,l} = 0$ to focus on the k-th spot.

To leading order, we then obtain a sequence of canonical problems

$$\frac{d}{dt}\phi_{k,l} = \frac{1}{n}\sum_{j \neq l}\frac{\phi_{k,l} - \phi_{k,j}}{|\phi_{k,l} - \phi_{k,j}|} + M_k\phi_{k,l} \tag{29}$$

where M_k is the same $d \times d$ constant matrix given by (12).

Consider K spots of equal size, symmetrically distributed along a ring. Such configurations are prevalent for certain force laws; an example is a force law as in Figure 1 with $(a, b) = (0.4, \ 0.1)$. In this case, since all the spots are symmetric, we fix an arbitrary $k = K$ with $x_K = (r, 0)$ and let $\phi_l = \phi_{K,l}$. Equation (29) then reduces to:

$$\frac{d}{dt}\phi_l = \frac{1}{n}\sum_{j \neq l}\frac{\phi_l - \phi_j}{|\phi_l - \phi_j|} - \begin{bmatrix} \alpha & 0 \\ 0 & \beta \end{bmatrix}\phi_l \tag{30}$$

where α, β are defined in (17, 18). For the special case $K = 3$ we obtain

$$\alpha = -a - \frac{3}{2}F'(d); \qquad \beta = -a - \frac{1}{2}F'(d)$$

where d is the inter-spot distance satisfying $F(d) = 0$.

Example. Take $F(r)$ as in Figure 1 with b replaced by δ so that

$$f(r) = \min(a + \delta/r, 1/r - 1) = \begin{cases} 1/r - 1, & r > \frac{1-\delta}{1+a} \\ a + \delta/r, & r < \frac{1-\delta}{1+a} \end{cases}.$$

Consider the case of four holes $K = 4$. When $\delta = 0$, we obtain from (14) that $r = 0.62132$ whenever $a > 0.1381$. From (17, 18) we then compute $\alpha = 1.8619 - a$; $\beta = 1.0572 - a$. Using Theorem 2.2, the four-hole solution is stable when $\delta = 0$ and $a = 0.3$. Next, take $a = 0.3, \delta = 0.03$. We then find $\beta/\alpha = 0.484$. The resulting four-spot equilibrium is shown in Figure 3. To validate this result, we compare this with the simulation of the *reduced system* (30) with $\alpha = 1$ and $\beta = 0.484$. Note how the reduced system preserves the shape of the original spot.

3.1   Analysis of the reduced problem (30)

We now concentrate on the system (30). Here, we are guided by observations in Figure 1. Note that some of the "spots" have very elongated shape; for example when $(a, b) = (0.2, 0.025)$, the spots appear to degenerate into small line segments. For other parameters such as $(a, b) = (0.6, 0.1)$ or as in Figure 3, the spots are fully two-dimensional and resemble ellipses. Below we show that the co-dimensionality of the spot can be understood in terms of the ratio β/α and the number n of particles within a spot in the reduced system (30).
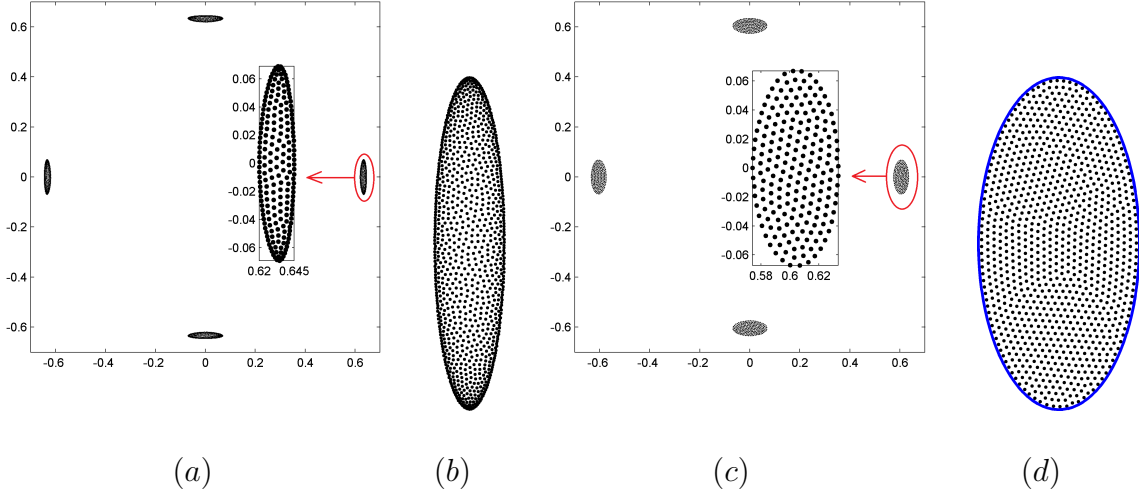
$$(a) \qquad\qquad (b) \qquad\qquad (c) \qquad\qquad (d)$$

Figure 3: (a) Steady state consisting of four spots for (2) with $N = 800$, $f(x) = \min(a + \delta/r, 1/r - 1)$, $a = 0.3$, $\delta = 0.05$. Insert shows the blowup of the spot. (b) Steady state of the reduced system (30) with $n = 1000, \alpha = 1, \beta = 0.484$. (c) Steady state consisting of four spots for (2) with $f(x) = \min(a + (\delta/r)^2, 1/r - 1)$, and N, a, δ as in (a). Insert shows the blowup of the spot. (d) Steady state of the reduced system (41) with $p = 2$, $n = 1000, \alpha = 1, \beta = 0.484$. The blue curve is the ellipse $(a\cos\theta, b\sin\theta)$ with a, b as given by Theorem 3.3.

To illustrate this phenomenon, fix the ratio $\beta/\alpha = 0.25$ and consider the evolution of (30) starting with random initial conditions for various values of n. This simulation is shown in Figure 4. For relatively small n, the steady state consists of a vertical line which is stable for $n \leq 30$. However this line is unstable when $n = 40$. As n is further increased, more bands appear until eventually the steady state starts to look like an elongated ellipse with principal axis ratio of around 0.025.

To simplify computations, we will represent vectors using complex numbers so that (30) becomes

$$\frac{d}{dt}\phi_l = \frac{1}{n}\sum_{j \neq l}\frac{\phi_l - \phi_j}{|\phi_l - \phi_j|} - \left(\frac{\alpha + \beta}{2}\phi_l + \frac{\alpha - \beta}{2}\bar{\phi}_l\right), \tag{31}$$

where $\bar{\phi}_l$ is the complex conjugate of ϕ_l.

We start with the observation that the system (31) admits the following "one-dimensional" solution. A straightforward check reveals that

$$\phi_l = \left\{\frac{2}{\beta n}l - \frac{1}{\beta}\left(1 + \frac{1}{n}\right)\right\}i, \qquad l = 1, 2, \ldots, n$$
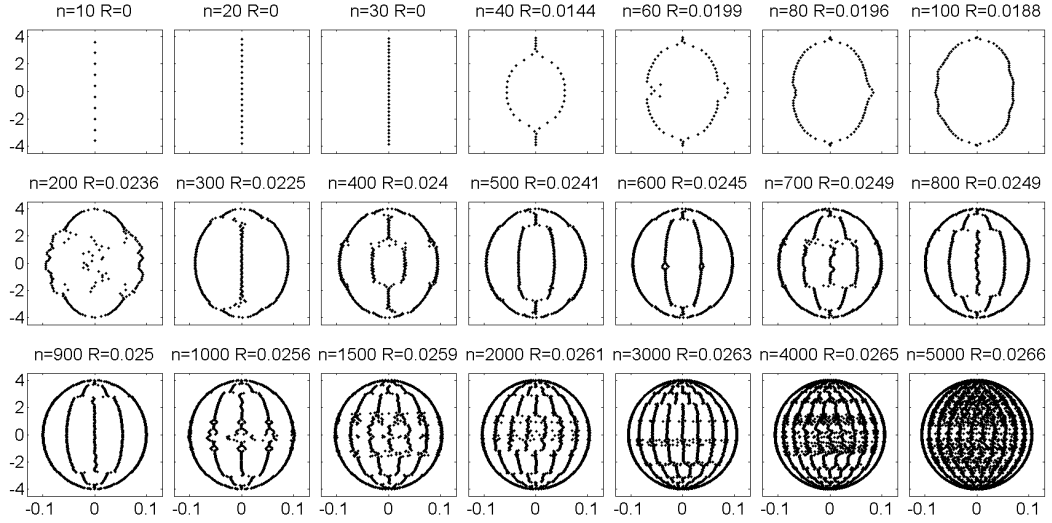
11

Figure 4: Steady states of the system (30) with $\beta/\alpha = 0.25$ and with n as indicated. Note that the horizontal axis is stretched out about 8 times in order to show better the structure of the steady state. The R in the caption is the ratio of the maximum horizontal displacement over the maximum vertical displacement.

is the exact steady state of (31). We next linearize around this steady state as

$$\phi_l(t) = \left\{ \frac{2}{\beta n}l - \frac{1}{\beta}\left(1 + \frac{1}{n}\right) \right\} i + \psi_l(t); \quad |\psi_l(t)| \ll 1.$$

After a lengthy computation we obtain

$$\frac{d}{dt}\psi_l = \sum_{j \neq l} \frac{\beta}{4\,|l-j|} \left[\bar{\psi}_l - \bar{\psi}_j + \psi_l - \psi_j \right] - \left(\frac{\alpha + \beta}{2}\psi_l + \frac{\alpha - \beta}{2}\bar{\psi}_l \right). \qquad (32)$$

The solution space to (32) factors into a direct product of the two subspaces: $\mathrm{Im}(\psi_l) = 0$ for all l or $\mathrm{Re}(\psi_l) = 0$ for all l. This corresponds to perturbations in purely horizontal or vertical directions, respectively. For the vertical perturbations, substitute $\psi_l = ic_l e^{\lambda t}$ where c_l is a real number. This yields an eigenvalue $\lambda = -\beta$ of multiplicity n. Thus the perturbation in the vertical direction is stable provided that $\beta > 0$. For the horizontal perturbation, we obtain the system

$$\frac{d}{dt}\psi_l = \sum_{j \neq l} \frac{\beta}{2\,|l-j|} \left[\psi_l - \psi_j \right] - \alpha\psi_l. \qquad (33)$$

The stability of this system follows from the following key lemma:

12

Lemma 3.1 *Consider the eigenvalue problem*

$$\lambda\psi_l = \sum_{\substack{j=1\ldots n \\ j\neq l}} \frac{\psi_l - \psi_j}{|l-j|}, \qquad l = 1\ldots n. \tag{34}$$

The n eigenvalues are given by $\lambda_k = 2S_k$, $k = 0\ldots n-1$ where $S_k = \sum_{j=1}^{k} \frac{1}{j}$ is the k-th harmonic number, with the convention that $S_0 = 0$.

The proof of this lemma is given below; it immediately follows that the eigenspace corresponding to (33) is given by

$$\lambda_k = (\beta S_k - \alpha), \qquad k = 0\ldots n-1. \tag{35}$$

Since S_k is an increasing positive sequence, the horizontal perturbations are stable if and only if

$$\beta S_{n-1} - \alpha < 0.$$

We summarize our funding as follows.

Theorem 3.2 *Consider the reduced system (30), and suppose that $\alpha, \beta > 0$. It admits the steady state consisting of particles located uniformly along a vertical line of length $2/\beta$, centered at the origin. Such steady state is stable provided that*

$$\sum_{j=1}^{n-1} \frac{1}{j} < \frac{\alpha}{\beta}, \tag{36}$$

and is unstable if the inequality is reversed. In the limit of large n, the inequality (36) is asymptotically equivalent to

$$n < \exp(\alpha/\beta - \gamma) \approx 0.5614\exp(\alpha/\beta) \tag{37}$$

where $\gamma \approx 0.5772$ is the Euler constant.

From this theorem, it is clear that a line is an unstable equilibrium of (30) for sufficiently large n. On the other hand, if α/β is sufficiently large, such a line can still be stable even with very large n. For example, in Figure 4 we have $\exp(\alpha/\beta - \gamma) = 30.65$, so a single line is stable with $n \leq 30$ but is unstable otherwise. This is indeed confirmed by direct simulations as Figure 4 demonstrates. It also helps to explain why the spots in the shape of a line is commonly observed in numerical simulations. In addition, even when the vertical line is *unstable*, when β/α is small, the resulting spot has the form of a very skinny ellipse which appears to "inherit" the dimensions of the unstable line as is illustrated in Figure 4.

Proof of Lemma 3.1. First, consider the following continuum limit version of the problem (34):

$$\lambda\psi(x) = \int_0^1 \frac{\psi(x) - \psi(y)}{|x - y|}dy \tag{38}$$

We compute for any integer p:

$$
\begin{aligned}
\int_0^1 \frac{x^p - y^p}{|x - y|}dy &= \int_0^x \frac{x^p - y^p}{x - y} - \int_x^1 \frac{x^p - y^p}{x - y} \\
&= x^p\left(\int_0^1 \frac{1 - t^p}{1 - t}dt - \int_1^{1/x} \frac{1 - t^p}{1 - t}dt\right) \\
&= x^p\left(\left\{t + \frac{t^2}{2} + \ldots + \frac{t^p}{p}\right\}\Big|_0^1 - \left\{t + \frac{t^2}{2} + \ldots + \frac{t^p}{p}\right\}\Big|_1^{1/x}\right) \\
&= 2\left(1 + \frac{1}{2} + \ldots \frac{1}{p}\right)x^p + Q_{p-1}(x)
\end{aligned}
$$

where $Q_{p-1}(x) = -\sum_{j=0}^{p-1}\frac{x^j}{p-j}$ is a polynomial of degree $p - 1$. Thus there exists some polynomial $R_{p-1}(x)$ of degree $p - 1$ such that

$$\psi_p = x^p + R_{p-1}(x); \qquad \lambda_p = 2\left(1 + \frac{1}{2} + \ldots \frac{1}{p}\right)$$

is an eigenfunction/eigenvalue pair.

This shows that λ_p are also the eigenvalues of the discrete problem (34), at least in the limit $n \to \infty$. In fact, $\lambda_0 \ldots \lambda_{n-1}$ are *exactly* the eigenvalues of the problem (34). This follows by the same argument as for the continuous problem, along with the fact that $\sum_1^n i^p = n^{p+1}/(p + 1) + Q_p(n)$ where $Q_p(n)$ is some polynomial of degree p. ∎

A direct application of the results from [8] shows that the steady state of the reduced system (30) is *confined* in the limit $n \to \infty$, whenever $\alpha, \beta > 0$: that is, the density of the steady state has compact support. However the precise shape of the steady state remains an open problem. Recently, Bernoff et.al. [3] have studied a class of aggregation models of the form (1) for the general case where $F(r)$ is smooth with $0 < F(0) < \infty$. Their analysis includes, as a special case, the reduced problem (30) when $\alpha = \beta$, which corresponds to $F(r) = 1 - r$. They found that near the edge of the swarm, the density has a profile of the form $\rho(x) = O(1/\sqrt{d})$ where d is the distance from the swarm's edge. We expect that their analysis can be generalized when $\alpha \neq \beta$.

3.2 Elliptical spots of uniform density

We now extend the analysis of §3 to more general singularly perturbed repulsion. We suppose that (27) is replaced by

$$f(r) \sim \delta r^{-p} + a + o(1), \quad 0 < r \ll 1, \quad 0 < \delta \ll 1, \quad p > 0; \tag{39}$$

so that (27) corresponds to the special case $p = 1$ of (39). As before, we assume that a steady state consisting of K holes located at $\{x_1, \ldots, x_K\}$ is stable when $\delta = 0$. Then we replace (28) by

$$x_{k,l}(t) = x_k + \delta^{1/p} \phi_{k,l}(t), \qquad \delta \ll 1. \tag{40}$$

For K equal holes along a ring, the reduced problem (30) then generalizes to

$$\frac{d}{dt}\phi_l = \frac{1}{n} \sum_{j \neq l} \frac{\phi_l - \phi_j}{|\phi_l - \phi_j|^p} - \begin{bmatrix} \alpha & 0 \\ 0 & \beta \end{bmatrix} \phi_l, \qquad l = 1 \ldots n \tag{41}$$

where as before, $n = N/K$ and α, β are defined as before in (17, 18). The case $p = 2$ corresponds to Newtonian repulsion in two dimensions; when $\alpha = \beta$, this problem was analysed in detail in [16, 6]. The continuum limit $n \to \infty$ of (41) with $p = 2$ is

$$\rho_t(x, t) + \nabla_x \cdot (v(x)\rho(x, t)) = 0; \tag{42}$$

$$v = \int_{\mathbb{R}^2} \{\nabla_x \ln |x - y| - A(x - y)\} \rho(y)\, dy, \qquad A = \begin{bmatrix} \alpha & 0 \\ 0 & \beta \end{bmatrix}.$$

Here, $\rho(x, t)$ represents the density of the particles and $v(x, t)$ is the velocity field. The following theorem describes a basic steady state of (42).

Theorem 3.3 *Define*

$$a := \sqrt{\frac{2}{\alpha + \beta} \frac{\beta}{\alpha}}; \qquad b := \sqrt{\frac{2}{\alpha + \beta} \frac{\alpha}{\beta}} \tag{43}$$

and let $D \subset \mathbb{R}^2$ be the ellipse of semi-axes a, b whose boundary is parameterised by $(a \cos \theta, b \sin \theta)$, $\theta \in [0, 2\pi]$. The system (42) admits an equilibrium state for which $\rho(x)$ is constant inside D and is zero outside D.

An example of this theorem is given in Figure 3(d), which shows the steady state of the particle system (41). The blue curve is the corresponding ellipse of Theorem 3.3. Excellent agreement with numerics is observed.

Proof of Theorem 3.3. As in [16, 6], we make use of the method of characteristics to describe the evolution. The characteristics for (42) are

$$\frac{d}{dt}x = v; \qquad \frac{d}{dt}\rho = -(\nabla \cdot v)\rho$$

and we compute

$$\nabla \cdot v = \int_{\mathbb{R}^2} \{\Delta_x \ln |x - y| - A\Delta_x |x - y|^2\} \rho(y)\, dy$$

$$= \int_{\mathbb{R}^2} \{2\pi\delta(x - y) - (\alpha + \beta)\} \rho(y)\, dy$$

$$= 2\pi\rho(x) - (\alpha + \beta) M$$

15

where M is the conserved mass

$$M = \int_{\mathbb{R}^2} \rho(y) dy.$$

Thus we have

$$\frac{d}{dt}\rho = ((\alpha + \beta) M - 2\pi\rho) \rho \tag{44}$$

so that the density evolves along characteristics independent of the specific location. Suppose that the initial conditions are

$$\rho(x, 0) = \begin{cases} \rho_0, & x \in D_0 \\ 0, & x \notin D_0 \end{cases}$$

where D_0 is some closed set. Then (44) implies that

$$\rho(x, t) = \begin{cases} \rho(t), & x \in D(t) \\ 0, & x \notin D(t) \end{cases} \tag{45}$$

where $\rho(t)$ is the solution to (44) subject to $\rho(0) = \rho_0$, and with $\rho(t) \to \frac{(\alpha+\beta)M}{2\pi}$ as $t \to \infty$. The evolution equations transport the initial support D_0 into a set $D(t)$ and the density remains constant inside that set, and zero outside. Thus the evolution of the original problem reduces to computing the evolution of the domain $D(t)$. Next we use the divergence theorem to compute:

$$v(x) = \left\{ \rho(t) \int_{D(t)} -\nabla_y \ln |x - y| \, dy \right\} - Ax \, |D(t)| \, \rho(t) \tag{46}$$

$$= -\frac{\rho(t)}{2} \left\{ \int_{\partial D(t)} \ln |x - y|^2 \, \hat{n} dS(y) \right\} - Ax \, |D(t)| \, \rho(t). \tag{47}$$

For a steady state solution, we have $\rho(x) = \frac{(\alpha+\beta)M}{2\pi}$ for all $x \in D$, and $v(x) = 0$ for all $x \in D$. Conversely, suppose that

$$v(x) = 0 \text{ for all } x \in \partial D, \quad \text{and} \quad \rho(x) = \begin{cases} \frac{(\alpha+\beta)M}{2\pi}, & x \in D \\ 0, & x \notin D \end{cases}. \tag{48}$$

Then from (46) we obtain $\nabla \cdot v = 0$; it follows that $v = 0$ for all $x \in \partial D$. Thus the necessary and sufficient conditions for ρ given by (45) to be a steady state are

$$\int_{\partial D(t)} \ln |x - y|^2 \, \hat{n} dS(y) = 2Ax \, |D| \, ; \text{ for all } x \in \partial D \qquad \text{and} \qquad (\alpha + \beta) \frac{|D|}{2\pi} = 1. \tag{49}$$

Suppose that D is an ellipse whose boundary is given by $y = (a \cos(\theta), b \sin(\theta))$. Write $x = (a \cos \phi, b \cos \phi) \in \partial D$. We will now show by a direct computation that conditions (49) are satisfied when a, b are given by (43). Using the identity

$$|x - y|^2 = a^2 (\cos \theta - \cos \phi)^2 + b^2 (\sin \theta - \sin \phi)$$

$$= 4a^2 \left(\sin \frac{\theta - \phi}{2} \sin \frac{\theta + \phi}{2} \right)^2 + 4b^2 \left(\sin \frac{\theta - \phi}{2} \cos \frac{\theta + \phi}{2} \right)^2$$

16

we find explicitly $\int_{\partial D(t)} \ln |x - y|^2 \, \hat{n} dS(y) = (I_x, I_y)$ with

$$I_x = b \int_0^{2\pi} \cos\theta \ln \left[4a^2 \left(\sin\frac{\theta - \phi}{2} \sin\frac{\theta + \phi}{2} \right)^2 + 4b^2 \left(\sin\frac{\theta - \phi}{2} \cos\frac{\theta + \phi}{2} \right)^2 \right] d\theta;$$

$$I_y = a \int_0^{2\pi} \sin\theta \ln \left[4a^2 \left(\sin\frac{\theta - \phi}{2} \sin\frac{\theta + \phi}{2} \right)^2 + 4b^2 \left(\sin\frac{\theta - \phi}{2} \cos\frac{\theta + \phi}{2} \right)^2 \right] d\theta.$$

We separate $I_x = bI_1 + bI_2$ with

$$I_1 = \int_0^{2\pi} \cos\theta \ln \left[4 \left(\sin\frac{\theta - \phi}{2} \right)^2 \right] d\theta;$$

$$I_2 = \int_0^{2\pi} \cos\theta \ln \left[a^2 \left(\sin\frac{\theta + \phi}{2} \right)^2 + b^2 \left(\cos\frac{\theta + \phi}{2} \right)^2 \right] d\theta.$$

and simplify

$$I_2 = \int_0^{2\pi} \cos\theta \ln \left[a^2 + b^2 + (b^2 - a^2) \cos(\theta + \phi) \right] d\theta$$

Now integration by parts followed by contour integration yields

$$\int_0^{2\pi} \cos(\theta - \phi) \ln(\alpha + \cos\theta) d\theta = \int \frac{\sin(\theta - \phi)}{\alpha + \cos(\theta)} d\theta, \quad |\alpha| > 1$$

$$= 2\pi \cos\phi \frac{\alpha}{|\alpha|} \left(|\alpha| - \sqrt{\alpha^2 - 1} \right)$$

and

$$\int_0^{2\pi} \cos(\theta) \ln \left[4 \left(\sin\frac{\theta - \phi}{2} \right)^2 \right] d\theta = \int_0^{2\pi} \cos(2\theta + \phi) \ln \left[\sin^2\theta \right] d\theta$$

$$= -2\pi \cos\phi$$

Suppose

$$b > a.$$

Then

$$I_x = 2\pi b \cos\phi \left(-1 + \frac{b^2 + a^2}{b^2 - a^2} - \sqrt{\left(\frac{b^2 + a^2}{b^2 - a^2} \right)^2 - 1} \right).$$

A similar computation yields

$$I_y = 2\pi b \sin\phi \left(-1 + \frac{b^2 + a^2}{b^2 - a^2} - \sqrt{\left(\frac{b^2 + a^2}{b^2 - a^2} \right)^2 - 1} \right)$$

so that $\int_{\partial D(t)} \ln |x - y|^2 \, \hat{n} dS(y) = (\cos\phi, \sin\phi) K$ where K is a constant. On the other hand, $Ax = (a\alpha \cos\phi, b\beta \sin\phi)$; so that the first equation in (49) becomes $(a\alpha \cos\phi, b\beta \sin\phi) = (\cos\phi, \sin\phi) K_2$ for some constant K_2. This is possible iff $\frac{b}{a} = \frac{\alpha}{\beta}$. The second equation in (49) then becomes $(\alpha + \beta) ab = 2$. Solving for (a, b) we then obtain the formula (43). ∎

4 Annulus solutions

In this section we study thin annular steady states, such as shown in Figure 1 for $(a, b) = (0.2, 0.2)$. As was demonstrated in [21], such steady states can arise in the neighbourhood of an ill-posed ring equilibrium. A ring equilibrium corresponds to a solution that concentrates uniformly on a circle; that is a degenerate annulus whose inner and outer radii are the same. A ring is *ill-posed* if it is unstable with respect to high-mode perturbations: that is, in the continuum limit, there are infinitely many positive (i.e. unstable) eigenvalues of the corresponding linearized problem; it is *well-posed* if at most finite number of eigenvalues are positive. The well-posedness of a ring was characterized in [21, 28]. In particular, it was shown that $F(0) = 0$ is one of the necessary conditions for the well-posedness. Here, we consider the case

$$f(r) = f_0(r) + \frac{\delta}{r} \quad \text{with} \ \ 0 < \delta \ll 1 \tag{50}$$

where f_0 is such that there is a stable ring solution when $\delta = 0$. In particular, f_0 must is bounded so that $F(0) = \delta$. An example of such a force is a perturbed quadratic force $F(r) = r - r^2 + \delta$ which corresponds to

$$f(r) = 1 - r + \frac{\delta}{r}; \qquad f_0(r) = 1 - r; \tag{51}$$

when $\delta = 0$, the stability of the ring was shown in [21].

Let R be the radius of the ill-posed ring (with $\delta > 0$). In the continuum limit, it satisfies

$$0 = \int_0^{\pi/2} f(2R \sin \theta) \sin^2(\theta) d\theta. \tag{52}$$

The annulus that forms will have a thin width of radius approximately R. To compute its precise dimensions as well as its radial profile, consider the hydrodynamic limit of (2) given by (3). We show the following asymptotic result.

Main Result 4.1 *Suppose that $f(r)$ is given by (50). Let R be the positive root of (52). Define*

$$K_{021} := 4 \int_0^{\pi/2} f_0 \left(2R \sin \theta \right) + 2R \sin^3 \theta f_0' \left(2R \sin \theta \right) d\theta$$

$$\beta := 16Re^{-2} \exp \left(\frac{K_{021} R}{2\delta} \right);$$

Suppose that $K_{021} < 0$ and that when $\delta = 0$, the system admits a stable ring solution of the radius R. Then for $0 < \delta \ll 1$, the system (3) has a steady state of the form of

18

$\delta = 0.35$ $\delta = 0.35$ $\delta = 0.2$
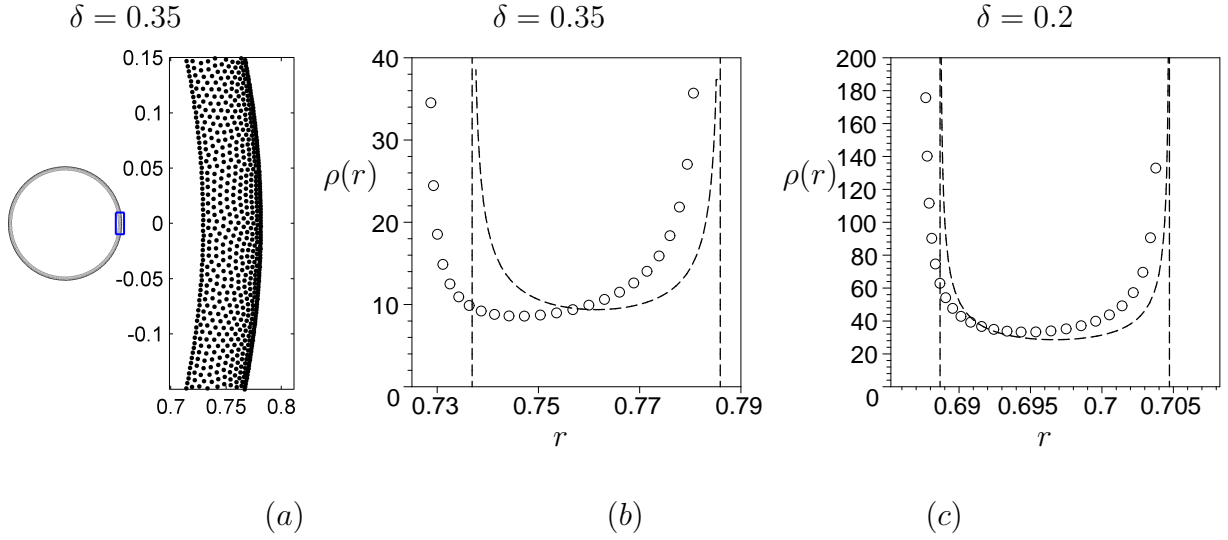
(a) (b) (c)

Figure 5: (a) The steady state of (2) in the form of an annulus for $f(r) = 1 - r + \frac{\delta}{r}$ with $N = 10,000$ and $\delta = 0.35$. Forward Euler method was used starting with random initial conditions. Output at time $t = 4000$ is shown. A zoomed in figure of the blue region reveals the non-uniform density. (b) The radial profile of the density in the continuum limit. Dots show the result of numerical simulation using the method of characteristics for the continuous limit. Dashed line shows the asymptotic prediction given by 53. (c) Same as (b) but with $\delta = 0.2$.

an annulus whose inner radius is $R_1 = R - \beta$ and whose outer radius is $R_2 = R + \beta$. Moreover the corresponding density inside the annulus is given to leading order by

$$\rho(x) \sim \begin{cases} \dfrac{c}{\sqrt{\beta^2 - (R - |x|)^2}}, & |R - x| < \beta \ll 1 \\ 0, & otherwise \end{cases} \qquad (53)$$

Example. Consider $f(r)$ given by (51). Then from (52), R satisfies

$$0 = 16R^2 - 3\pi R - 6\delta \implies$$

$$R = \frac{3\pi}{32} + \frac{3\pi}{32}\sqrt{1 + \frac{128\delta}{3\pi^2}} \sim \frac{3\pi}{16} + \frac{2}{\pi}\delta + O(\delta^2).$$

We then compute

$$K_{021} = 2\pi - \frac{40R}{3} < 0;$$

$$\beta = 16Re^{-2}\exp\left(-\frac{R}{\delta}\left(\frac{20R}{3} - \pi\right)\right)$$

$$\sim 3\pi e^{-5}\exp\left(-\frac{3\pi^2}{64\delta}\right) \qquad (54)$$

19

Taking $\delta = 0.35$ yields $\beta = 0.024511$; the annulus has inner and outer radii $(R_1, R_2) = (0.73691, .78593)$. To validate the asymptotic results, we have used the method of characteristics to numerically solve (3) for radially symmetric steady state using the method described in [16]. This method much more precise than solving the full particle model (2) since the radial symmetry is utilized to reduce the dimension of the problem, and allows us to obtain accurate results even for small values of δ. We found a very good agreement between the numerics and asymptotics as shown in Figure 5.

Derivation of Main Result 4.1. We seek a radially symmetric solution. Write $\vec{v} = v(r)(\cos\theta, \sin\theta)$ and we obtain

$$v(r) = \int_0^\infty K(s, r)\rho(s)s\,ds \tag{55}$$

where

$$K(s, r) := \int_0^{2\pi} (r - s\cos\theta) f\left(\sqrt{r^2 + s^2 - 2rs\cos\theta}\right) d\theta. \tag{56}$$

We assume that the annulus is very thin, so that $v = 0$ when r is far from R. With this in mind, we expand (56) as

$$r = R + \xi, \quad s = R + \eta; \quad \xi, \eta \ll 1.$$

The precise scaling for ξ, η will be shown later to be exponentially small in δ. We further split K as $K = K_0 + \delta K_1$ where

$$K_0 := 2\int_0^\pi (r - s\cos\theta) f_0\left(\sqrt{r^2 + s^2 - 2rs\cos\theta}\right) d\theta$$

$$K_1 := 2\int_0^\pi (r - s\cos\theta)\left(r^2 + s^2 - 2rs\cos\theta\right)^{-1/2} d\theta$$

We start by computing K_1. Write $K_1(s, r) = g(r/s)$ where

$$g(t) := 2\int_0^\pi (t - \cos\theta)\left(1 + t^2 - 2t\cos\theta\right)^{-1/2} d\theta.$$

Suppose that $t = 1 + \varepsilon$. Then expanding, we have

$$g(1 + \varepsilon) \sim 4 - 2\varepsilon\ln|\varepsilon| + \varepsilon\left(6\ln 2 - 2\right) + O(\varepsilon^2\ln|\varepsilon|)$$

Setting $r = R + \xi$, $s = R + \eta$; then we obtain

$$K_1(r, s) \sim g\left(1 + \frac{\xi - \eta}{R}\right)$$

$$\sim 4 - 2\frac{\xi - \eta}{R}\ln|\eta - \xi| + \frac{\xi - \eta}{R}\left(2\ln 8R - 2\right).$$

20

Next we compute K_0. We expand

$$r - s\cos\theta = 2R\sin^2\frac{\theta}{2} + 2\eta\sin^2\frac{\theta}{2} - \eta + \xi$$

$$\sqrt{r^2 + s^2 - 2rs\cos\theta} \sim 2R\sin\frac{\theta}{2} + (\xi + \eta)\sin\frac{\theta}{2}$$

and expand K_0 as $K_0 \sim K_{01} + K_{02}$ where K_{01} is $O(1)$ and K_{02} is $O(\xi, \eta)$:

$$K_{01} = 8R\int_0^{\pi/2} f_0\left(2R\sin\theta\right)\sin^2\theta d\theta;$$

$$K_{02} = 4\int_0^{\pi/2} f_0\left(2R\sin\theta\right)\left(2\eta\sin^2\theta - \eta + \xi\right) + 2R\sin^2\theta f_0'\left(2R\sin\theta\right)\sin\theta\left(\xi + \eta\right)d\theta.$$

Further expand

$$K_{02} = K_{021}\xi + K_{022}\eta$$

where

$$K_{021} = 4\int_0^{\pi/2} f_0\left(2R\sin\theta\right) + 2R\sin^3\theta f_0'\left(2R\sin\theta\right)d\theta$$

$$K_{022} = 4\int_0^{\pi/2} f_0\left(2R\sin\theta\right)\left(2\sin^2\theta - 1\right) + 2R\sin^2\theta f_0'\left(2R\sin\theta\right)\sin\theta d\theta.$$

Finally using the equation (52) for R we get

$$K(s,r) \sim \alpha_1\xi + \alpha_2\eta - 2\delta\frac{\xi - \eta}{R}\ln|\eta - \xi|\,.$$

where

$$\alpha_1 = K_{021} + \frac{\delta}{R}\left(2\ln 8R - 2\right); \qquad \alpha_2 = K_{022} - \frac{\delta}{R}\left(2\ln 8R - 2\right).$$

Changing variables $s = R + \eta;\quad \rho(s) = \varrho(\eta)$, the equation (55) then becomes

$$v \sim \int_{-R}^{\infty}\left\{\alpha_1\xi + \alpha_2\eta - 2\delta\frac{\xi - \eta}{R}\ln|\eta - \xi|\right\}\varrho(\eta)\left(R + \eta\right)d\eta$$

We assume that the annulus has inner radius R_1 and outer radius R_2, so that $v = 0$ when $r \in (R_1, R_2)$. We shift the coordinates so that $v = 0$ for $\eta \in (a, \beta)$ where we define

$$\alpha = R_1 - R; \quad \beta = R_2 - R.$$

In addition, we assume $\eta \ll 1$. Then the condition $v = 0$ becomes

$$\int_\alpha^\beta\left\{\alpha_1\xi + \alpha_2\eta - 2\delta\frac{\xi - \eta}{R}\ln|\eta - \xi|\right\}\varrho(\eta)d\eta \sim 0; \quad \xi \in (\alpha, \beta) \tag{57}$$

Differentiating with respect to ξ, this becomes

$$\int_\alpha^\beta \ln|\eta - \xi|\, \varrho(\eta)d\eta = \int_\alpha^\beta \left\{ \frac{\alpha_1 R}{2\delta} - 1 \right\} \varrho(\eta)d\eta; \qquad \xi \in (\alpha, \beta) \tag{58}$$

This is an integral equation for $\rho(\xi)$, with the right and side being a constant. It is a special case of the so-called Carleman's equation whose full solution is given as formula 3.4.2 in [25]. We first seek symmetric solution with $\alpha = -\beta$. From [25] we find that the only possible solution is a constant multiple of

$$\varrho(\eta) = \frac{1}{\sqrt{\beta^2 - \eta^2}}.$$

The left hand side of (58) then evaluates to

$$\int_{-\beta}^\beta \frac{\ln|\eta - \xi|}{\sqrt{1 - \eta}}d\eta = \pi \ln \beta - \pi \ln 2; \qquad |\xi| < \beta.$$

and for the right side of (58) we get

$$\int_{-\beta}^\beta \left\{ \frac{\alpha_1 R}{2\delta} - 1 \right\} \varrho(\eta)d\eta = \left\{ \frac{\alpha_1 R}{2\delta} - 1 \right\} \pi$$

so that

$$\beta \sim \exp\left(\frac{\alpha_1 R}{2\delta} - 1 + \ln 2 \right).$$

It remains to show that $\alpha = -\beta$. This is done by plugging the anzatz $\varrho(\eta) = \frac{1}{\sqrt{(\beta - \eta)(\eta - \alpha)}}$ directly into (57) and collecting the terms in ξ. Self-consistency of the anzatz then leads to $\alpha = -\beta$. $\blacksquare$

4.1 Newtonian perturbation

We now construct annular solutions which arise when a small Newtonian repulsion is added to a force that has a stable ring as its steady state. That is, we consider (2) with $f(r)$ given by

$$f(r) = f_0(r) + \frac{\delta}{r^2}. \tag{59}$$

where $f_0(r)$ is the same as in §4; for example $f_0(r) = 1 - r$. Let R_0 be the radius of the ring steady state with $\delta = 0$, that is,

$$0 = \int_0^{\pi/2} f_0(2R_0 \sin \theta) \sin^2(\theta)d\theta. \tag{60}$$

22

$\delta = 0.0125$ $\delta = 0.00625$ $\delta = 0.00625$
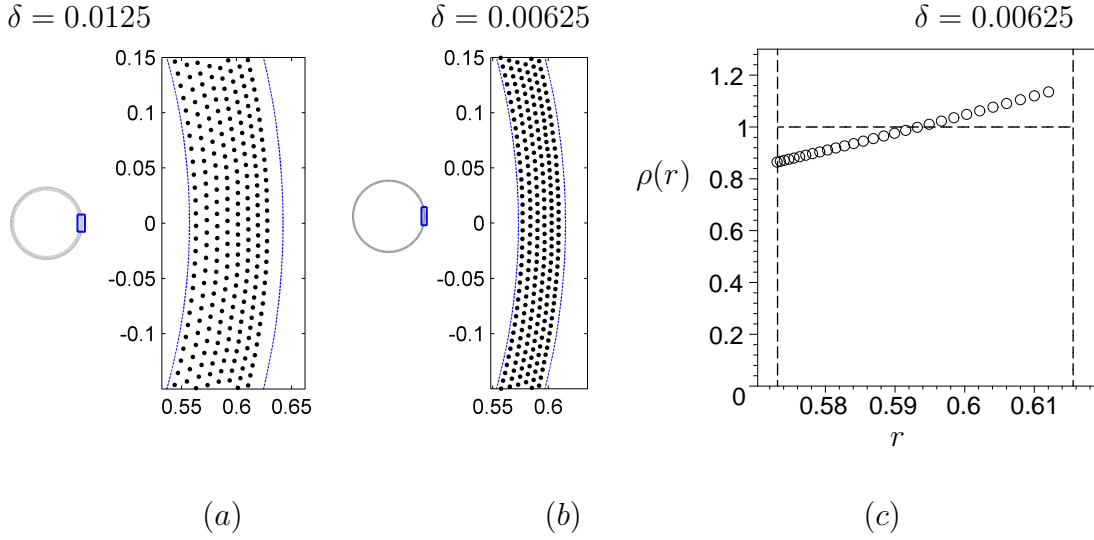
(a) (b) (c)

Figure 6: (a) The steady state of (2) in the form of an annulus for $f(r) = 1 - r + \frac{\delta}{r^2}$ with $N = 3,000$ and $\delta = 0.0125$. Forward Euler method was used starting with random initial conditions. Output at time $t = 4000$ is shown. Blue dashed lines show the asymptotic boundaries of the annulus R_1, R_2 as given by (65). (b) Same as (a) except with $\delta = 0.00625$. (c) The radial profile of the density in the continuum limit with $\delta = 0.00625$. Dots show the result of numerical simulation using the method of characteristics for the continuum problem. Dashed line shows the asymptotic prediction given by (65).

As before, we expand asymptotically the vector field

$$v(r) = \int_0^\infty K(s, r)\rho(s)s\, ds$$

where

$$K(s, r) := \int_0^{2\pi} (r - s\cos\theta)\, f\left(\sqrt{r^2 + s^2 - 2rs\cos\theta}\right) d\theta. \tag{61}$$

Split K as $K = K_0 + \delta K_1$ where

$$K_0 := 2\int_0^\pi (r - s\cos\theta)\, f_0\left(\sqrt{r^2 + s^2 - 2rs\cos\theta}\right) d\theta$$

$$K_1 := 2\int_0^\pi (r - s\cos\theta)\left(r^2 + s^2 - 2rs\cos\theta\right)^{-1} d\theta$$

We compute

$$\int_0^\pi (t - \cos\theta)\left(1 + t^2 - 2t\cos\theta\right)^{-1} d\theta = \begin{cases} 0, & 0 < t < 1 \\ \pi/t, & t > 1 \end{cases}$$

so that

$$K_1(s, r) = \begin{cases} 0, & r < s \\ \dfrac{2\pi}{r}, & r > s \end{cases}.$$

23

Next, we compute K_0 by expanding around R_0 as

$$r = R_0 + \xi; \quad s = R_0 + \eta; \quad \xi, \eta = O(\delta).$$

As in §4 we then find

$$v(r) \sim \int_0^\infty \left(K_{021} \left(r - R \right) + K_{022} \left(s - R \right) \right) \rho(s) s \, ds + \frac{\delta 2\pi}{r} \int_0^r \rho(s) s \, ds$$

where

$$K_{021} = 4 \int_0^{\pi/2} f_0 \left(2R_0 \sin \theta \right) + 2R_0 \sin^3 \theta \, f_0' \left(2R_0 \sin \theta \right) d\theta$$

$$K_{022} = 4 \int_0^{\pi/2} -f_0 \left(2R_0 \sin \theta \right) + 2R_0 \sin^3 \theta \, f_0' \left(2R_0 \sin \theta \right) d\theta.$$

Assume that $R_0 + \alpha, R_0 + \beta$ are the interior and exterior radii of the annulus, respectively, with $\alpha, \beta \ll 1$. Changing the variables $r - R = \xi, s - R = \eta, \ \rho(r) = \varrho(\xi)$, we obtain

$$0 \sim \int_\alpha^\beta \left(K_{021} \xi + K_{022} \eta \right) \varrho(\eta) R_0 d\eta + \delta 2\pi \int_\alpha^\xi \varrho(\eta) d\eta, \quad \xi \in (\alpha, \beta). \tag{62}$$

Differentiating (62) we then obtain

$$2\pi \delta \varrho(\xi) = -R_0 K_{021} \int_\alpha^\beta \varrho(\eta) d\eta. \tag{63}$$

This implies that ϱ is a constant for $\xi \in (\alpha, \beta)$. Without loss of generality, take $\varrho = 1$ so that (62) becomes

$$K_{021} \xi R_0 \left(\beta - \alpha \right) + \frac{1}{2} K_{022} R_0 \left(\beta^2 - \alpha^2 \right) + 2\pi \delta \left(\xi - \alpha \right) = 0, \quad \xi \in (\alpha, \beta)$$

Equating coefficients of ξ finally yields the annulus dimensions

$$\alpha = \frac{K_{022} \pi}{R_0 K_{021} \left(K_{022} + K_{021} \right)} \delta; \quad \beta = -\frac{\left(K_{022} + 2K_{021} \right) \pi}{R_0 K_{021} \left(K_{022} + K_{021} \right)} \delta. \tag{64}$$

Example: We take $f(r) = 1 - r + \delta/r^2$. Then $f_0(r) = 1 - r$ and we obtain $R_0 = \frac{3}{16}\pi$; $K_{021} = -\pi/2$; $K_{022} = -3\pi/2$; $\alpha = -\frac{8}{\pi}\delta$; $\beta = \frac{40\delta}{3\pi}$. This yields the inner and outer radius of

$$R_1 = \frac{3}{16}\pi - \frac{8}{\pi}\delta; \quad R_2 = \frac{3}{16}\pi + \frac{40\delta}{3\pi}. \tag{65}$$

Figure 6 shows that an excellent agreement is observed between the asymptotics and the full numerics of the continuum limit (42).

5   Discussion

A simple piecewise-linear force (4) is all it takes to generate a rich class of steady states as seen in Figure 1. In this paper we have shown that many of these states can be understood of in terms of singular perturbations of lower dimensional patterns: spots arise as bifurcations of point clusters; annuli are perturbations of a ring. Asymptotic methods provide a powerful tool to describe the stability, shape and precise dimensions of these complex patterns. Spots and annuli form basic building blocks from which it is possible to construct more complex solutions, such as multiple annuli, soccer balls, and hybrid spot-annulus patterns. We are currently investigating how to combine these basic blocks into more complex patterns.

Many open problems remain. Consider the reduced problem (30). Based on numerical evidence of Figure 4, we conjecture that in the limit $N \to \infty$, the steady state is an ellipse whenever $\alpha, \beta > 0$. Note that for the problem (41) with $p = 2$, we showed this explicitly in Theorem 3.3. But the problem (30) is more difficult since the density is non-constant: even for the radially symmetric case $\alpha = \beta$, the precise density profile is unknown (although it was shown in [3] that the density blows up near the boundary in this case). We have described the profile of the annulus under the perturbation (39) with $p = 1$ or $p = 2$. An interesting open problem is to describe the ring profile for a more general case, $0 < p < 2$. Finally, many questions remain for three and higher dimensions. For example, numerical simulations of (30) in three dimensions indicate that the equilibrium density concentrates on the surface of what looks like an ellipsoid. In the case $\alpha = \beta$, it was shown in [28] that the equilibrium density indeed concentrates on the surface of a sphere. The more general case $\alpha \neq \beta$ remains open.

References

[1] D. BALAGUE, J. A. CARRILLO, T. LAURENT, AND G. RAOUL, *Nonlocal interactions by repulsive-attractive potentials: radial ins/stability*, Submitted, Physica D.

[2] N. BELLOMO AND F. BREZZI, *Traffic, crowds, and swarms*, Math. Models Methods Appl. Sci., 18 (2008), pp. 1145–1148.

[3] A. BERNOFF AND ET.AL., *In preparation.*

[4] A. J. BERNOFF AND C. M. TOPAZ, *A primer of swarm equilibria*, SIAM Journal on Applied Dynamical Systems, 10 (2011), pp. 212–250.

[5] A. L. BERTOZZI, J. A. CARRILLO, AND T. LAURENT, *Blow-up in multidimensional aggregation equations with mildly singular interaction kernels*, Nonlinearity, 22 (2009), pp. 683–710.

[6] A. L. BERTOZZI, T. LAURENT, AND F. LEGER, *Aggregation and spreading via the newtonian potential: The dynamics of patch solutions*, to appear in M3AS, (2012).

[7] A. L. Bertozzi, T. Laurent, and J. Rosado, L^p *theory for the multidimensional aggregation equation*, Comm. Pure Appl. Math., 64 (2011), pp. 45–83.

[8] J. A. Carrillo, M. DiFrancesco, A. Figalli, T. Laurent, and D. Slepčev, *Global-in-time weak measure solutions and finite-time aggregation for nonlocal interaction equations*, Duke Math. J., 156 (2011), pp. 229–271.

[9] J. A. Carrillo, M. R. D'Orsogna, and V. Panferov, *Double milling in self-propelled swarms from kinetic theory*, Kinet. Relat. Models, 2 (2009), pp. 363–378.

[10] I. D. Couzin and J. Krause, *Self-organization and collective behavior of vertebrates*, Adv. Study Behav., 32 (2003), pp. 1–67.

[11] F. Cucker and S. Smale, *Emergent behavior in flocks*, IEEE Trans. Automat. Control, 52 (2007), pp. 852–862.

[12] M. R. D'Orsogna, Y. L. Chuang, A. L. Bertozzi, and L. S. Chayes, *Self-propelled particles with soft-core interactions: Patterns, stability, and collapse*, Phys. Rev. Lett., 96 (2006), p. 104302.

[13] R. Eftimie, G. de Vries, and M. A. Lewis, *Complex spatial group patterns result from different animal communication mechanisms*, Proc. Natl. Acad. Sci. USA, 104 (2007), pp. 6974–6979 (electronic).

[14] R. Erban and H. G. Othmer, *From individual to collective behavior in bacterial chemotaxis*, SIAM J. Appl. Math., 65 (2004/05), pp. 361–391 (electronic).

[15] K. Fellner and G. Raoul, *Stable stationary states of non-local interaction equations*, Math. Models Methods Appl. Sci., 20 (2010), pp. 2267–2291.

[16] R. C. Fetecau, Y. Huang, and T. Kolokolnikov, *Swarm dynamics and equilibria for a nonlocal aggregation model*, Nonlinearity, 24 (2011), pp. 2681–2716.

[17] J. Haile, *Molecular Dynamics Simulation: Elementary Methods*, John Wiley and Sons, Inc., New York, 1992.

[18] T. Hillen, *Hyperbolic models for chemosensitive movement*, Math. Models Methods Appl. Sci., 12 (2002), pp. 1007–1034. Special issue on kinetic theory.

[19] D. D. Holm and V. Putkaradze, *Aggregation of finite-size particles with variable mobility*, Phys Rev Lett., 95:226106 (2005).

[20] ——, *Formation of clumps and patches in self-aggregation of finite-size particles*, Physica D., 220 (2006), pp. 183–196.

[21] T. Kolokolnikov, H. Sun, D. Uminsky, and A. L. Bertozzi, *Stability of ring patterns arising from two-dimensional particle interactions*, Phys. Rev. E, 84 (2011), p. 015203.

[22] H. Levine, W.-J. Rappel, and I. Cohen, *Self-organization in systems of self-propelled particles*, Phys. Rev. E, 63 (2000), p. 017101.

[23] R. Lukeman, Y. Li, and L. Edelstein-Keshet, *Inferring individual rules from collective behavior*, Proc. Natl. Acad. Sci. USA, 107 (2010), pp. 12576–12580.

[24] A. Mogilner and L. Edelstein-Keshet, *A non-local model for a swarm*, J. Math. Biol., 38 (1999), pp. 534–570.

[25] A. D. Polyanin and A. V. Manzhirov, *Handbook of integral equations*, Chapman & Hall/CRC, Boca Raton, FL, second ed., 2008.

[26] C. Topaz, A. Bernoff, S. Logan, and W. Toolson, *A model for rolling swarms of locusts*, Euro. Phys. J., 157 (2008), pp. 93–109.

[27] G. Toscani, *One-dimensional kinetic models of granular flows*, M2AN Math. Model. Numer. Anal., 34 (2000), pp. 1277–1291.

[28] J. von Brecht, D. Uminsky, T. Kolokolnikov, and A. Bertozzi, *Predicting pattern formation in particle interactions*, to appear, M3AS.

[29] J. H. von Brecht and D. Uminsky, *On soccer balls and linearized inverse statistical mechanics*, J. Nonlin. Sci, to appear, (2012).